Chemical Papers (2020) 74:3467–3474
https://doi.org/10.1007/s11696-020-01183-5

ORIGINAL PAPER

Nanomechanical characterization of electrospun biodegradable vascular scaffolds

Emel Berna Yilmaz[1] · Sinan Eğri[1] · Özlem Eğri[1] · Mustafa Oguzhan Caglayan[2]

Received: 21 October 2019 / Accepted: 2 May 2020 / Published online: 7 May 2020

Abstract

We proposed a method to determine the mechanical properties of electrospun nanofibers intended for use in vascular tissue engineering. Mechanical properties of poly(L-lactide) and poly(ε-caprolactone) copolymers and blends which are in fiber form were tested using the nanoindentation technique. Individual nanofibers were prone to give overweighed distributions in terms of *E* moduli in indentation testing. An increased compressive elastic modulus of 17 MPa was obtained in case of an increasing amount of poly(ε-caprolactone) in the fibers. It has also been found that the Hertzian model of compression is not adequate to model the elastic deformation of individual fibers.

Keywords Vascular scaffolds · Electrospun nanofiber · Nanoindentation · Compressive elastic modulus

Introduction

The efficacy of vascular scaffolds used in tissue engineering depends on biocompatibility and the mechanical properties approaching natural veins (Gao et al. 2019; Mitchell and Niklason 2003). A vascular scaffold should ensure optimal adaptation to the mechanical behavior of tissue and should not interfere with normal changes in surrounding tissues by producing undesirable reactions (inflammation, clot formation, etc.) in the tissue (Fraser et al. 2006). Mechanical properties of a vascular scaffold must be strong enough to perform mechanical functions, even if they are not the same as the replacement tissue. In addition, the scaffold must resist the loading forces until the primary tissue matures (Hollister et al. 2005; Hutmacher 2000).

Mechanical properties of the vascular grafts, such as elastic modulus, have the potential to affect long-term vessel patency and determine the strength of the graft in the tissue (Qiu and Tarbell 1996). It has been reported that, due to the sudden variations in blood pressure, a vascular graft should withstand cyclic loadings and has a burst strength above 260 kPa (L'Heureux et al. 2007). Reported uniaxial tensile elastic moduli for human blood vessels are between 5 and 100 MPa (Hasan et al. 2014).

Poly L-lactic acid (PLLA) and poly ε-caprolactone (PLC) have been widely used in the fabrication of vascular grafts (Janmohammadi and Nourbakhsh 2019; Zhang et al. 2014). Especially nano/microfibers of these polymers and their copolymers have been preferred due to their unique advantages in vascular graft production (Ekaputra et al. 2008; He et al. 2009; Ju et al. 2010). The electrospinning process is based on the high electrostatic force spinning to produce nano/microfibers from viscoelastic solutions of polymers/copolymers (Agarwal et al. 2008). Electrospun fibers can be produced in many morphological combinations by changing the affecting parameters such as electrical conductivity, viscosity and flow rate of the polymer solution, as well as environmental and physicochemical factors (Ferrari et al. 2017; Soliman et al. 2011). For example, an increase in solute concentration or viscosity results with an increase in the fiber diameter, as well as a decrease in the porosity. Electrospinning has become a key production method for PLLA- and PCL-based vascular grafts since it has dozens of controllable production parameters and results in almost

Electronic supplementary material The online version of this article (https://doi.org/10.1007/s11696-020-01183-5) contains supplementary material, which is available to authorized users.

✉ Mustafa Oguzhan Caglayan
oguzhan.caglayan@bilecik.edu.tr

[1] Department of Bioengineering, Gaziosmanpaşa University, Tokat, Turkey

[2] Department of Bioengineering, Bilecik Seyh Edebali University, Bilecik, Turkey

uniform final nano/microfibrous product (Ferrari et al. 2017; Vurugonda et al. 2018; Weijie et al. 2016).

In the relevant literature, there is a limited number of studies on the mechanical properties of biomaterials used in vascular applications. The studies, in which mechanical tests were performed on woven vascular grafts such as woven PU (Li et al. 2007) and PLA (Li et al. 2017) with universal test devices, can be found in the literature. Mechanical properties of nanofibrous vascular grafts made of PLLA/PCL blend have been determined by conventional tensile testing, and it was reported that the elastic modulus (100% PLLA, 170 MPa) decreased to 33 MPa by increasing the amount of PCL to 10% (Henry et al. 2017). It has been reported that the ultimate strength of the electrospun ε-caprolactone heparin-coated matrices (1–2.5 MPa) has been determined only by macro-mechanical tests (Gong et al. 2016). However, no work has been found reporting the comparative nanomechanical characterization of electrospun vascular grafts made of PLLA, PCL, their blends and their copolymers.

There are various studies related to vascular grafts. For instance, by using electrospun polyethylene glycol dimethacrylate (PEGDMA), the mechanical behavior of dry and hydrated grafts has been investigated and authors stated that the elastic modulus which was initially 350 kPa decreased in the hydrated state between 2 and 18 kPa (Wingate et al. 2012). In another vascular scaffold application, authors reported that the strength of the cellulose acetate propionate matrix, which contained cellulose nanocrystals (3% by mass), had been increased (Pooyan et al. 2012). Biomechanical behavior of the aortic wall (E approx. 100–150 kPa) has also been investigated by using a semi-linear viscoelastic modeling approach in three dimensions (Kermani et al. 2017). Elastic properties of arteriovenous fistula in mice have been determined using AFM nanoindentation (Laurito et al. 2016). The authors stated that the elastic modulus of the mouse vein varied between 4.4 and 17.7 kPa and the hardness of the arteries could be determined in various regions. In another nanomechanical test performed using AFM, the mechanical properties of the subendothelial matrix of the bovine carotid artery have been investigated and the elastic modulus of 2.7 kPa was reported (Peloquin et al. 2011). Mechanical properties of various electrospun scaffolds for vascular grafts have been collected and reported in a review paper (Hasan et al. 2014).

In this study, a method for the investigation of the mechanical properties of the vascular biomaterial obtained by the electrospinning method is presented. So far, nanoindentation and its modified counterparts have not been used for the determination of mechanical properties of individual nanofibers. We proposed a Hertzian contact model and suggested some modifications as an alternative to the macro-mechanical tests in determining the mechanical strength of the submicron-sized individual fibers obtained by electrospinning.

Experimental

General

ε-Caprolactone monomer was purchased from Merck (Germany) and used as received. L-lactide (Purasorb L®) dimer was purchased from Corbion (The Netherlands) and used after recrystallization in toluene. Stannous octoate ($SnOct_2$) was purchased from Sigma-Aldrich (USA) and used as received for catalysis of polymerization reactions. All other chemicals that were used are analytical grade and were purchased from the local representative of Sigma-Aldrich (USA) company. In all stages, deionized pure water was used for washing and rinsing purposes. All water solutions have been prepared by using ultrapure water. AFM cantilevers have been purchased from a local representative of Park Systems Company (Korea), and specifications stated by the manufacturer were used in modulus calculations.

Polymerization

The first stage of polymerization was carried out at 115 °C by purging the dimer-monomer mixture with N_2. The catalyst ($Sn(Oct)_2$, 0.1% by weight) was added to the reaction medium, then the medium was held at constant reaction temperature (120 °C) for 24 h. After the reaction complete, the medium was then dissolved with chloroform. Methanol at − 20 °C was used to precipitate the solubilized fraction. After the precipitation in methanol, the product was dried under vacuum at 30 °C to remove methanol and residual chloroform. The product obtained was stored at − 20 °C. Depending on the PLA/PCL proportions of the polymer, produced blends were labeled as B1 (70/30), B2 (60/40) and B3 (50/50), and copolymers produced were labeled as C1 (70/30), C2 (60/40) and C3 (50/50).

Electrospinning

New Era Systems NE-300 model electrospinning device was used. Optimal parameters have been selected according to optimization results, such as the distance between the collector and syringe tip (130 mm), polymer/solution ratio (10% (g/mL)), the applied voltage (20 kV), the syringe size and injection rate (20 gauge and 3 mL/h). Polymer fibers were deposited on a rotary collector arranged as horizontal assembly, under the specified conditions. Electrospun fibers were maintained at − 20 °C for nanomechanical tests. Molecular weights of the polymers were determined using the Ostwald

viscometer at 25 °C, according to Mark Houwink's relation (Rolf 2004; Wang et al. 1998).

FTIR and SEM analysis

Attenuated total reflection-Fourier transform infrared spectrometer (ATR-FTIR) analyses of the produced copolymers were carried out using the Bruker Eco ATR model FTIR instrument. For ATR-FTIR measurements, ZnSe prism was used, and the spectrum was recorded between 400 and 4000 cm^{-1}. Electron microscopy images were taken by MIRA3 TESCAN instrument. For this purpose, electrospun specimens were placed on a sample disk and dried at 45 °C in a vacuum environment. Subsequently, specimens were coated with Au (approx. 15 nm) under vacuum. SEM images were obtained at between 2 and 50 kX magnification. The relative standard deviation (RSD%) value for the mean particle size and size distribution was determined by the evaluation of SEM graphs with open-source image processing software.

Nanomechanical tests with AFM

Nanomechanical tests were conducted using the ParkSystem XE-100 model AFM device which was placed in a climate-controlled room held at 21 °C. Electrospun specimens and AFM tips have been used as-is. In this study, the Hertzian contact model was used, in which the polymer fiber has been compressed by an external mechanical load with the AFM tip. In order to reduce the complexity of modeling the contact behavior between the AFM tip and the microfiber, indentation data acquired from the upper part of the microfiber were used. The load applied in this way results in uniaxial compression. In addition, it was assumed that the particle volume did not change because of the extent of the compression load and the depth of the indentation. The Hertzian contact model takes into account the contact deformation of elastic materials under normal loads in the absence of adhesion and friction and is also widely used in nanostructure tests (Sánchez-Arévalo et al. 2017). The elastic modulus, Poisson's ratio, arc constant, tip diameter and a cone angle of the AFM tip used in all experiments were 130 GPa, 0.27, 0.6 N/m, 8 nm and 40°, respectively.

Results and discussion

Molecular weight and FTIR characterization

Molecular weights of PLA and PCL were in the range of 70–80 kDa. While the caprolactone monomer ratio in the reaction content increased from 30 to 50% by weight, the molecular weights of copolymers decreased gradually from 40 to 20 kDa (See section S.1 in the Supplementary document).

C-H stretching peaks of PLA were observed around wavenumbers 2996 cm^{-1} and 2945 cm^{-1}, and C–H bending bands were observed around wavenumbers 1455 cm^{-1} and 1360 cm^{-1}. Stretching bands of C–O in ester bonding were resident around wavenumbers 1180 cm^{-1} and 1081 cm^{-1}. The peak observed at 1749 cm^{-1} belongs to C=O stretching of the carbonyl group in the neighborhood of the ester bonding between repeating units. C–H stretching peaks of PCL were observed at 2941 cm^{-1} and 2865 cm^{-1}, and C–H bending bands were observed around wavenumbers 1455 cm^{-1} and 1354 cm^{-1}. C=O stretching of the carbonyl group was observed at 1720 cm^{-1}. The main indicator in the FTIR spectra for successful polymerization of both PLA and PCL is the C=O stretching peaks (1749 cm^{-1} for PLA and 1721 cm^{-1} for PCL) observed for carbonyl group resident in the ester bonding. Comparing the copolymers using different ratios of lactide dimer to caprolactone monomer, as this ratio increased in the favor of lactide a broader peak laying between 1749 and 1721 cm^{-1}. C–H stretching peaks were weaker in intensity for the PLA, and stronger for PCL. As the dimer ratio increased, the intensity of the C–H stretching bands of the copolymers observed to be weakened. According to FTIR results, polymerizations for PLA and PCL and copolymerizations with indicative ratios of lactide and caprolactone were confirmed.

SEM characterization

SEM images of PLA, PCL, polymer blends and copolymers are given in Fig. 1. It can be said that PLA fibers were uniform and did not contain electrospinning defects such as agglomeration. PLA fiber diameter distribution was between 0.5 and 1.5 μm (see section S.3 in the Supplementary document). According to the image analysis, the non-normalized orientation distribution was in two directions, but the distribution of these directions wasn't dominant compared to the other directions (see section S.4 in the Supplementary document). In PCL images, the size distribution was smaller than PLA and the uniformity of the diameter on the single fiber was slightly lower. PCL fibers have had a smaller and rather narrow size distribution. The mean diameter of the PCL fibers was about 120–150 nm and the overall distribution was between 50 and 300 nm. Moreover, it can be said that there is a concentrated orientation in two directions. The diameter distribution of B1 was around 700 nm due to co-spinning, and also caused a slight distribution below 500 nm depending on the amount of PCL in the polymer, which may be evidence of phase separation or flaws in co-spinning. Furthermore, unlike PLA and PCL, large-diameter fibers reaching 2 μm were also observed. Nanofiber structures formed with different diameters for B2 are shown in Fig. 1. It can be

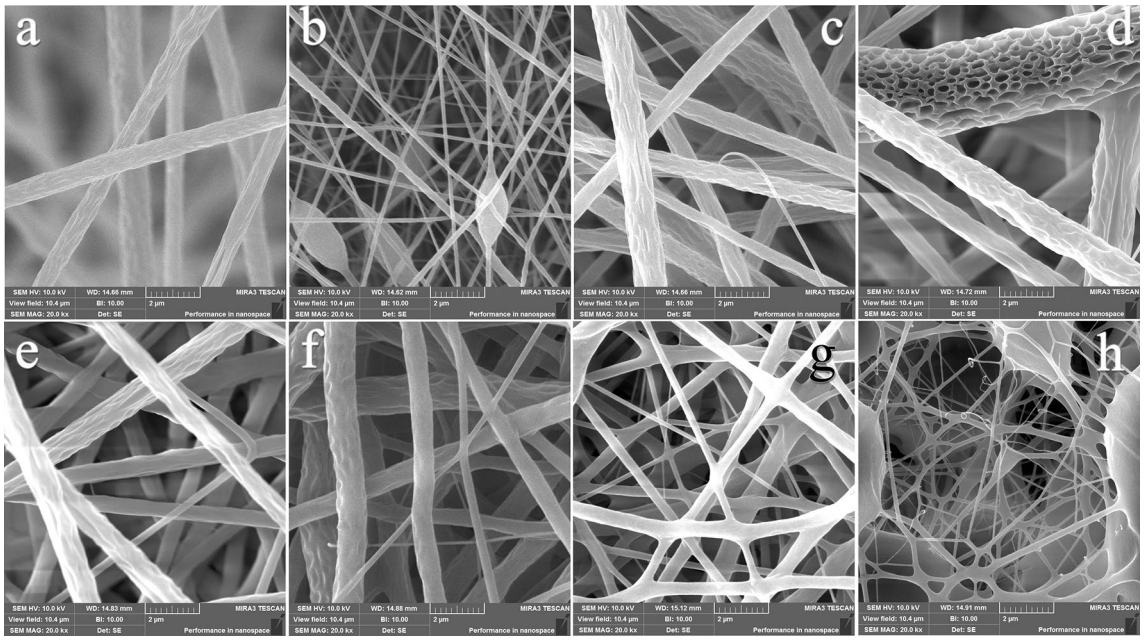

Fig. 1 SEM images for electrospun **a** PLA, **b** PCL, **c**–**e** polymer blends and **f**–**h** copolymers

seen that large-diameter fibers having surface defects. The size analysis of B2 showed a significant size distribution ranging from 1 to 2 μm due to the wider fibers with surface flaws, and a very large-diameter distribution between 1000 and 500 nm, similar to the B1 mixture. The orientation distribution analysis of B2 fibers revealed that the orientation was random. The B3 fibers were produced with a relatively more uniform diameter compared to the B2 fibers. Particularly large and porous fibers that have been observed in B2 fibers were not found in this sample. A uniform diameter distribution obtained for B3 was very similar to B1 fibers. The distribution of fiber diameters was below 1000 nm as in the B1 and B2. In addition, large-diameter fibers up to 1.6 μm were found. The orientation distribution of the B3 samples was approximately similar to B1.

Unlike polymer blends, junction zones were observed for C1 in the regions where the fibers overlap. The stresses caused by the connection between the fibers emerge from the curved junctions. The individual fibers have had higher diameters at connection points with other fibers. The C1 nanofiber size distribution gave two overweighed zones at approximately 400 nm and 800 nm. Similarly, the distribution of large-diameter (> 1.5 μm) fibers obtained in the B2 and B3 fibers was more pronounced in the C1 fibers. Considering the orientation frequency, a more frequent distribution was observed in three directions, but a high frequency and continuous distribution were obtained in the intermediate directions. Therefore, it can be said that the fibers having two orientations result in a very wide orientation due to the curvature of the regions in which they form connections. It is seen that the fibers of the C2 form a connection with each other and that the fiber diameters increased at these connection points, and that the tension of the fibers at the connection points leads to arcuate connections. However, due to the small number of connection points, the size distribution was quite uniform. Unlike the B1–B3 and C1 samples, the size distribution of less than 900 nm was particularly concentrated in the 200–300 nm band. Similar to the other samples, the size distribution was about 600 nm. In the direction distribution, there were three different direction distributions which were especially narrow. Similar to C1, the presence of anchor points and therefore the formation of curved forms led to a large direction distribution. Considering the SEM images of the C3 fibers, they have had more than one anchor point resulting in a network like formation. As in the case of C2 fibers, nodes were formed in the connection points of the fibers. These nodes were not porous, as seen in C2 fibers. Fiber diameters were found to be lower. The size distribution of copolymer C3 was 0–300 nm and relatively uniform. In particular, fibers having a diameter of less than 100 nm were dominant in the distribution. The C3 copolymer shows a high orientation in two directions. Although there was a large frequency distribution in other directions due to the connection points, there were also large diameters of fibers with a bi-directional distribution.

Nanoindentation

In the 5 μm × 5 μm scan areas, a minimum of 15 randomized indentations was performed. The compression

elastic modulus was calculated according to the Hertzian contact model, using the characteristic mechanical properties of the AFM tip declared by the manufacturer. Because of the extremely soft and flexible structure of the samples, AFM topography images were noisy, so it was not possible to evaluate the surface properties (particle distribution, roughness, etc.).

Compression elastic modulus results obtained from multiple points and different regions of the sample are presented as distribution histograms. As expected, fibers of different diameters that were in contact with each other randomly distributed multiple support points, transmitted and distributed the applied load. Therefore, a compression module with a much wider distribution was obtained when it was compared with the bulk material results using AFM (Caglayan 2017). The compression elastic modulus (E) is presented in the logarithmic axis so that the distribution can be seen clearly (Fig. 2).

E modulus of PCL was in between 0.3 and 10 MPa, with two main distribution regions at 300–1000 kPa and 3–10 MPa. E modulus of PLA fibers up to 100 kPa has had a distribution with a central log$E$ of 1.5, which corresponds to a compression module of about 30 kPa. The compression elastic modulus distribution of the fibers of the B1 mixture was in between the log$E$ 2.0–3.0 (300 kPa–1 MPa). There was also a lower-frequency distribution around 2–3 kPa. The nanomechanical test result of the fibers of the B2 blend gave log$E$ between 3.0 and 4.5 (1–30 MPa). The B3 specimen has had a very narrow distribution between log E 2.5–3.0 (300 kPa–1 MPa). Similar to the results of the B1 and B2 blends, there was also a very low-frequency distribution at 3–30 kPa compared to the overall modulus distribution. The compression modulus distribution of the C1 specimen was in the range of 5–10 MPa. When C2 copolymer fibers were examined, a high-frequency distribution around 500 kPa as well as a low-frequency distribution around 5 kPa was observed. The compression elastic modulus of C3 shows a narrower distribution compared to the other copolymer samples (10–22 MPa with a peak maximum of 16 MPa). Since the diameter distributions of the nanofibers have been wide in most cases in this study, frequency comparisons were statistically performed using distribution graphs to discuss and compare the specimens. Morphological and mechanical properties of specimens are given in Fig. 3 as the mid-frequency data according to the distribution frequency analysis.

The average diameter of PLA and PCL fibers was 830 nm and 135 nm, respectively, B1 and B2 have had approximately the same diameter in the polymer blends. The average size of B3 blend with a high PCL ratio was slightly smaller than B1 and B2 (625 nm). Radical size changes occurred in copolymers. All copolymers gave two distinct diameter distributions observed at a distribution frequency of 30% or more. As the PCL ratio increased, the diameters of the copolymer fibers gradually decreased from 875 to 175 nm (about PCL diameter). The second diameter distribution region was 225 nm for C1 and 55 nm for the C3 sample.

The compression elastic modulus of the produced fibers was compared by taking the peak value of the weighted frequency distribution (Fig. 3b). PLA fibers have had a lower compression module than PCL (42 kPa and 458 kPa respectively), in contrary to bulk material results (Henry et al. 2017). It was determined that PCL has behaved as a stiff component in the electrospun scaffold material. Surprisingly, the compression modulus of C1–C3 samples increased with the increasing amount of PCL in the copolymer. The C1 specimen had a low modulus compared to its precursor PLA and PCL. In the copolymers C2 and C3, the PCL ratio increased to 40% and the compression elastic modulus increased exponentially and reached about 900 kPa for C2 and 17 MPa for C3. Although it is clear that the increase in PCL content in the copolymer increases the strength of the electrospun material, which in turn a rapid increase in C2 and C3 might be as a result of the interconnected structure in the polymer fibers.

In order to ensure the suitability of the Hertzian model, the maximum force exerted by the indentation tip was limited so that the nanofiber would be subjected to elastic deformation only at the point where the force has been applied. In this ideal case, the reliability of the indentation measurements would be increased. However, according to given results (especially for C1–C3), network formation between nanofibers gave a much higher elastic modulus, which in turn suggests that the deformation resistance measured during the indentation process can be expressed by the modified version of the Hertzian model. As seen in Fig. 4, the Hertzian model for elastic deformation of a specimen can be explained as two resistances connected in series with elastic deformation of the AFM tip. However, in addition to the elastic deformation of interconnected fibers, there was an additional E3 module that represents the elastic bending of the fibers between the contact points.

Elastic deformation occurring on the sample surface when pressure is applied with the AFM tip includes both the elastic deformation of the surface and the elastic bending of the beam formed by the nanofiber between two or more anchor points. The system can, therefore, be modeled in series with an elastic deformation resistance E2, which is connected in parallel to an elastic flexural stiffness (E3) in the direction of the force. However, since the distance between the tip and each attachment point of each fiber is not known, the amount and the resistance of the bending due to the applied force cannot be determined. Consequently, the compression elastic modulus presented for the C2 and C3 nanofibers also includes an unknown amount of elastic flexural stiffness.

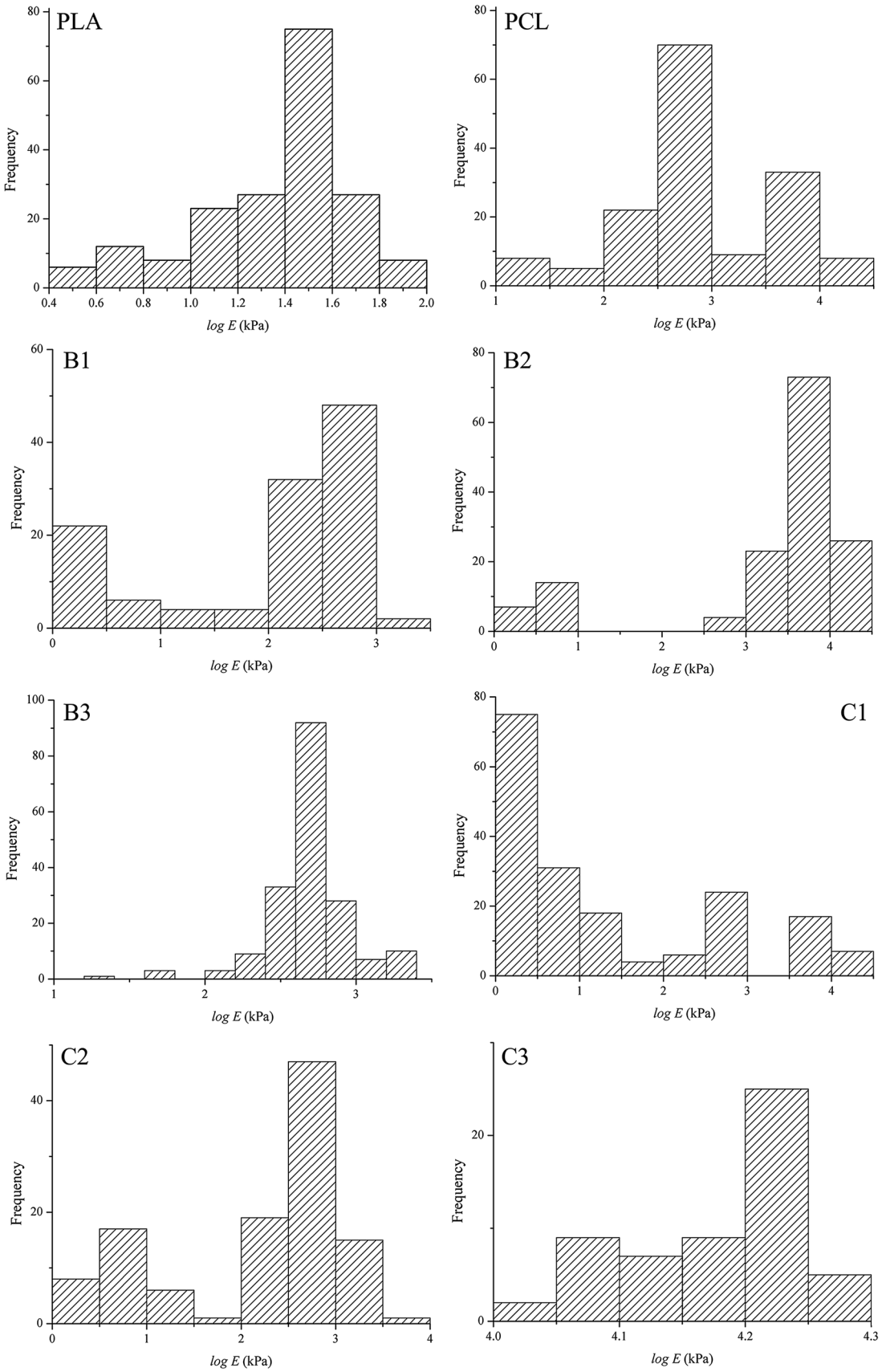

Fig. 2 Compression elastic modulus (*E*) histograms for PLA, PCL, polymer blends and copolymers

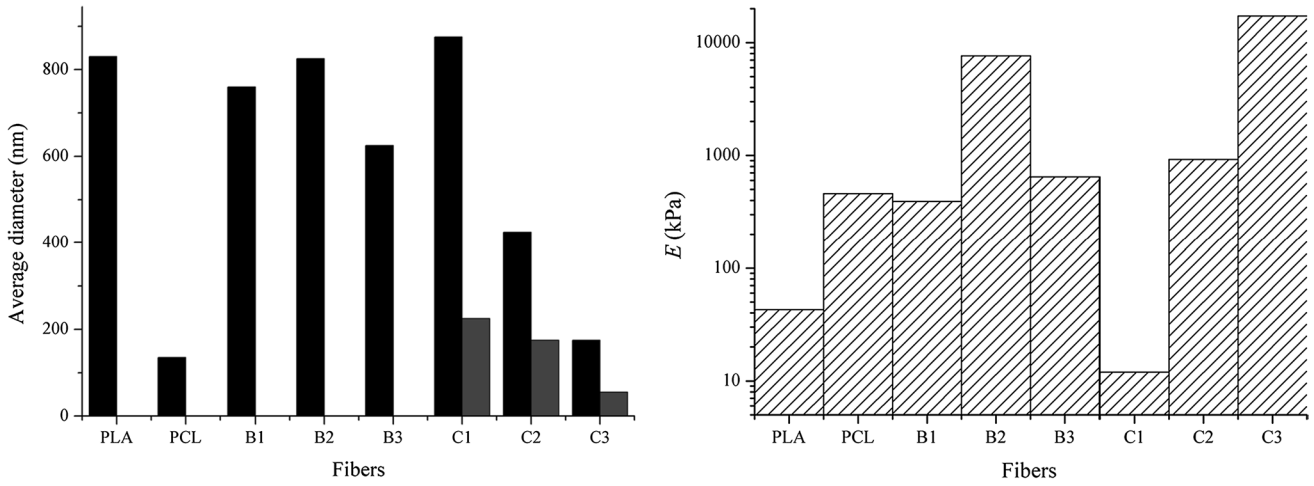

Fig. 3 Average size and compression elastic modulus of the specimens

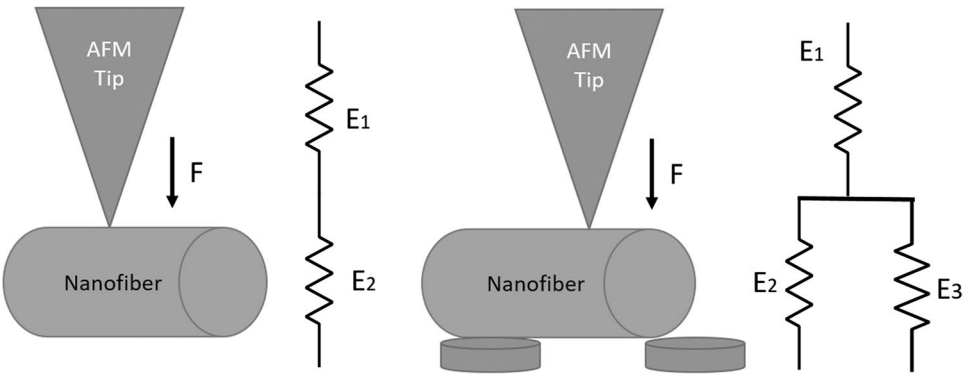

Fig. 4 The model of the Hertz model used in the nanoindentation process with Ohm's Law analogy (right), the modified Hertz model due to the possible bending in the structure (left)

Conclusions

The method proposed in this study gave repeatable and reliable but not exact compressive modulus results in the determination of the mechanical properties of electrospun nanofibers in tissue engineering. The compression elastic modulus that is lower than the bulk material is the result of the crystallization of the material associated with the production method and known/accepted by the researchers in this field. In the case of materials with large size distribution and uniformity, limiting the depth of indentation may reduce the systematic error in determining the nanomechanical behavior of the material. However, except for the shape change which can be expressed by the Poisson's ratio, additional elastic deformation resistances together with the change in shape make it difficult to make the results comparable. Also, in our case, beams produced by hanging fiber parts between contact points alter the results, due to additional elastic flexural deformation.

References

Agarwal S, Wendorff JH, Greiner A (2008) Use of electrospinning technique for biomedical applications. Polymer 49:5603–5621. https://doi.org/10.1016/j.polymer.2008.09.014

Caglayan MO (2017) Nanomechanical characterization of flowable dental restorative nanocomposite resins using AFM. Polym Plast Technol Eng 56:1813–1821. https://doi.org/10.1080/03602559.2017.1289409

Ekaputra AK, Prestwich GD, Cool SM, Hutmacher DW (2008) Combining electrospun scaffolds with electrosprayed hydrogels leads to three-dimensional cellularization of hybrid constructs. Biomacromolecules 9:2097–2103. https://doi.org/10.1021/bm800565u

Ferrari PF, Aliakbarian B, Lagazzo A, Tamayol A, Palombo D, Perego P (2017) Tailored electrospun small-diameter graft for vascular prosthesis. Int J Polym Mater Polym Biomater 66:635–643. https://doi.org/10.1080/00914037.2016.1252361

Fraser JK, Wulur I, Alfonso Z, Hedrick MH (2006) Fat tissue: an underappreciated source of stem cells for biotechnology. Trends Biotechnol 24:150–154. https://doi.org/10.1016/j.tibtech.2006.01.010

Gao J, Guo H, Tian S, Qiao Y, Han J, Li Y, Wang L (2019) Preparation and mechanical performance of small-diameter PHBHHx vascular

graft by electrospinning. Int J Polym Mater Polym Biomater 68:575–581. https://doi.org/10.1080/00914037.2018.1473865
Gong W et al (2016) Hybrid small-diameter vascular grafts: anti-expansion effect of electrospun poly ε-caprolactone on heparin-coated decellularized matrices. Biomaterials 76:359–370. https://doi.org/10.1016/j.biomaterials.2015.10.066
Hasan A et al (2014) Electrospun scaffolds for tissue engineering of vascular grafts. Acta Biomater 10:11–25. https://doi.org/10.1016/j.actbio.2013.08.022
He W, Ma Z, Teo WE, Dong YX, Robless PA, Lim TC, Ramakrishna S (2009) Tubular nanofiber scaffolds for tissue engineered small-diameter vascular grafts. J Biomed Mater Res Part A 90A:205–216. https://doi.org/10.1002/jbm.a.32081
Henry JJD, Yu J, Wang A, Lee R, Fang J, Li S (2017) Engineering the mechanical and biological properties of nanofibrous vascular grafts for in situ vascular tissue engineering. Biofabrication 9:035007. https://doi.org/10.1088/1758-5090/aa834b
Hollister SJ et al (2005) Engineering craniofacial scaffolds. Orthod Craniofac Res 8:162–173. https://doi.org/10.1111/j.1601-6343.2005.00329.x
Hutmacher DW (2000) Scaffolds in tissue engineering bone and cartilage. Biomaterials 21:2529–2543
Janmohammadi M, Nourbakhsh MS (2019) Electrospun polycaprolactone scaffolds for tissue engineering: a review. Int J Polym Mater Polym Biomater 68:527–539. https://doi.org/10.1080/00914037.2018.1466139
Ju YM, Choi JS, Atala A, Yoo JJ, Lee SJ (2010) Bilayered scaffold for engineering cellularized blood vessels. Biomaterials 31:4313–4321. https://doi.org/10.1016/j.biomaterials.2010.02.002
Kermani G, Hemmasizadeh A, Assari S, Autieri M, Darvish K (2017) Investigation of inhomogeneous and anisotropic material behavior of porcine thoracic aorta using nano-indentation tests. J Mech Behav Biomed Mater 69:50–56. https://doi.org/10.1016/j.jmbbm.2016.12.022
Laurito T et al (2016) Assessment of micro-mechanical variations in experimental arteriovenous fistulae using atomic force microscopy. J Vasc Access 17:279–283. https://doi.org/10.5301/jva.5000514
L'Heureux N, Dusserre N, Marini A, Garrido S, de la Fuente L, McAllister T (2007) Technology insight: the evolution of tissue-engineered vascular grafts-from research to clinical practice. Nat Clin Pract Cardiovasc Med 4:389–395. https://doi.org/10.1038/ncpcardio0930
Li X, An YH, Wu YD, Song YC, Chao YJ, Chien CH (2007) Microindentation test for assessing the mechanical properties of cartilaginous tissues. J Biomed Mater Res Part B Appl Biomater 80:25–31. https://doi.org/10.1002/jbm.b.30564
Li C, Wang F, Douglas G, Zhang Z, Guidoin R, Wang L (2017) Comprehensive mechanical characterization of PLA fabric combined with PCL to form a composite structure vascular graft. J Mech Behav Biomed Mater 69:39–49. https://doi.org/10.1016/j.jmbbm.2016.11.005
Mitchell SL, Niklason LE (2003) Requirements for growing tissue-engineered vascular grafts. Cardiovasc Pathol 12:59–64
Peloquin J, Huynh J, Williams RM, Reinhart-King CA (2011) Indentation measurements of the subendothelial matrix in bovine carotid arteries. J Biomech 44:815–821. https://doi.org/10.1016/j.jbiomech.2010.12.018
Pooyan P, Tannenbaum R, Garmestani H (2012) Mechanical behavior of a cellulose-reinforced scaffold in vascular tissue engineering. J Mech Behav Biomed Mater 7:50–59. https://doi.org/10.1016/j.jmbbm.2011.09.009
Qiu Y, Tarbell JM (1996) Computational simulation of flow in the end-to-end anastomosis of a rigid graft and a compliant artery. ASAIO J (Am Soc Artif Inter Organs 1992) 42:M702–M709
Rolf M (2004) Hermann Staudinger and the origin of macromolecular chemistry. Angew Chem Int Ed 43:1054–1063. https://doi.org/10.1002/anie.200330070
Sánchez-Arévalo FM, Muñoz-Ramírez LD, Álvarez-Camacho M, Rivera-Torres F, Maciel-Cerda A, Montiel-Campos R, Vera-Graziano R (2017) Macro- and micromechanical behaviors of poly(lactic acid)-hydroxyapatite electrospun composite scaffolds. J Mater Sci 52:3353–3367. https://doi.org/10.1007/s10853-016-0624-y
Soliman S, Sant S, Nichol JW, Khabiry M, Traversa E, Khademhosseini A (2011) Controlling the porosity of fibrous scaffolds by modulating the fiber diameter and packing density. J Biomed Mater Res Part A 96:566–574. https://doi.org/10.1002/jbm.a.33010
Vurugonda U, Rednam P, Sinha M (2018) Development of biodegradable scaffold using polylactic acid and polycaprolactone for cardiovascular application. Int J Polym Mater Polym Biomater 67:78–85. https://doi.org/10.1080/00914037.2017.1297945
Wang K, Huang H, Sheng J (1998) Determination of the Mark–Houwink equation parameters and their interrelationship. J Liq Chromatogr Relat Technol 21:1457–1470. https://doi.org/10.10826079808000527
Weijie Z et al (2016) Cistanche polysaccharide (CDPS)/polylactic acid (PLA) scaffolds based coaxial electrospinning for vascular tissue engineering. Int J Polym Mater Polym Biomater 65:38–46. https://doi.org/10.1080/00914037.2015.1055629
Wingate K, Bonani W, Tan Y, Bryant SJ, Tan W (2012) Compressive elasticity of three-dimensional nanofiber matrix directs mesenchymal stem cell differentiation to vascular cells with endothelial or smooth muscle cell markers. Acta Biomater 8:1440–1449. https://doi.org/10.1016/j.actbio.2011.12.032
Zhang W et al (2014) Preliminary study for vascular tissue engineering by electrospinning angelica polysaccharide (ASP)/PLA microfibrous scaffolds. Int J Polym Mater Polym Biomater 63:672–679. https://doi.org/10.1080/00914037.2013.854241